Magnetic dynamics in the disordered phases of condensed oxygen

1993 J. Phys.: Condens. Matter 5 423

(http://iopscience.iop.org/0953-8984/5/4/010)

J. Phys.: Condens. Matter 5 (1993) 423–442. Printed in the UK

Magnetic dynamics in the disordered phases of condensed oxygen

A Chahid†, F J Bermejo†, E Enciso‡, M García-Hernández† and J L Martínez§||

† Instituto de Estructura de la Materia, Consejo Superior de Investigaciones Cientificas, Serrano 123, E-28006 Madrid, Spain

‡ Departamento de Quimica-Fisica I, Facultad de Ciencias Quimicas Universidad Complutense-Madrid, E-28040, Madrid, Spain

§ Institut Laue–Langevin, 156X, F-38042 Grenoble Cédex, France

Received 4 September 1992, in final form 5 November 1992

Abstract. A high-resolution inelastic neutron scattering study of the liquid and plastic crystal phases of oxygen is presented. The separation of the magnetic response from the total cross sections is achieved by means of a computer molecular dynamics simulation which enables an approximate estimation of the magnetic spectral weight functions. The magnetic dynamics of the orientationally disordered plastic crystal is shown to exhibit a characteristic behaviour corresponding to an exchange-coupled paramagnet. The magnetic response of the liquid phase retains the most salient characteristics of the rotationally disordered solid phase.

1. Introduction

The magnetic properties of condensed oxygen have attracted a considerable attention since the early measurements of its static susceptibility by Kammerlingh-Onnes *et al* [1]. Contrary to monoatomic systems, the magnetic interactions have their origin in the direct coupling of molecular orbitals. As a consequence a strong interplay between the orientational lattice-dynamical and magnetic degrees of freedom is expected to occur in the low temperature solid phases.

At normal pressure and for temperatures up to 54.4 K condensed oxygen is a molecular solid, and three crystalline modifications (α, β and γ) take place within the solid range ($T_\alpha < 23.9$ K $< T_\beta < 43.8$ K $< T_\gamma < 54.4$ K).

The structure of the two lowest-temperature phases is well established from diffraction studies. The α phase is monoclinic (space group $C2/m$) [2] while the β phase is rhombohedral ($R\bar{3}m$) [3], both having one molecule per unit cell and showing long-range orientational order. The γ phase is cubic ($Pm\bar{3}n$) with eight molecules per unit cell [4] and is orientationally disordered. The liquid range at SVP conditions comprises temperatures between 54.4 K and 90.2 K and the triple and critical points are given respectively by ($T = 54.36$ K, $P = 1.52$ bar) and ($T = 154.58$ K, $P = 50.4$ bar).

|| Permanent address: Instituto de Ciencia de Materiales, CSIC, Facultad de Ciencias C-IV, Universidad Autónoma de Madrid, E-28049, Madrid, Spain.

0953-8984/93/040423+20$07.50

From magnetic susceptibility measurements [5], only the α phase has been found to show a long-range antiferromagnetic (AF) behaviour, whereas a two-dimensional AF order seems to exist in the β phase and both the γ phase and the liquid are macroscopically paramagnetic. From unpolarized neutron scattering studies [6] the existence of long-range AF order in the lowest-temperature phase has been confirmed, while the absence of clear magnetic Bragg reflections was interpreted in terms of the presence of short-range order. A coherence length of about 6 Å was postulated for the β phase, a fact which was later confirmed by a recent polarized neutron diffraction experiment [7].

While behaving as a paramagnet macroscopically, polarized neutron experiments have shown that the observed magnetic form factors for the γ phase and the liquid consistently deviate from simple paramagnetic behaviour [7]. Several models to account for the rotational disorder in the plastic-crystal phase have been proposed [6,7], and the widely accepted picture that emerges from such studies portrays the crystal as formed by two different kinds of molecules (as far as the orientational disorder is concerned). Two molecules of the unit cell are considered to be orientationally isotropic, whereas the remaining six are arranged as rotating within parallel disks along the crystal $C2$ axes.

Apart from polarized neutron diffraction studies [7] as well as a molecular dynamics simulation where only the structural aspects were considered [8], no other attempts to study the time-dependent properties of the liquid have been reported. A polarized inelastic neutron scattering study of the α and β phases was reported by Stephens [7], but to our knowledge these studies were not extended to analyse the dynamics of the orientationally disordered phases.

The purpose of the present work is to provide experimental evidence regarding the magnetic dynamics in both plastic-crystal and liquid phases of condensed oxygen. Some preliminary results have already been given [9,10] concerning the liquid phase and a comparison between the most salient features concerning the dynamics of this phase and the plastic crystal is given by means of the concurrent use of high-resolution unpolarized inelastic neutron scattering (INS) and computer molecular dynamics (MD) calculations. Although, in principle, the nuclear and magnetic scattering contributions can be separated by means of the use of full polarization analysis, such a procedure becomes extremely difficult to follow due to the relatively low magnetic scattering cross section of this material. In order to provide a means to separate both structural and magnetic responses, a MD calculation was carried out. Although such a procedure to separate both contributions has to be considered as approximate (neglects the coupling between magnetic and structural dynamics) it can be safely used to analyse the dynamics within the liquid and plastic-crystal phases, where contrary to the low-temperature phases, the magnetic correlations are known to be weak and spatially short-ranged. Several criteria may be adduced to validate this method of separation, and in particular, the procedure can be considered as adequate provided that

(i) the method can reproduce accurately the most salient features regarding the dynamic correlations of structural origin such as self-diffusion coefficients for the liquid phase, reorientational correlation times, frequencies of the collective excitations etc, and that

(ii) the approximation should reproduce the $S(Q,\omega)$ dynamic structure factors below 2 Å, where most of the observable intensity arises from structural effects.

On the other hand, the computer simulation can also be used to test the

importance of the rotation–translation coupling which could be important, especially in the solid phase.

The sketch of this paper is as follows, section 2 contains the relevant formulae used to express the structural and magnetic cross sections. The details concerning the experimental and molecular dynamics calculations are given in section 3, and the results from the analysis of the MD trajectories are given in section 4. The analysis of the experimental spectra once the structural contributions have been subtracted is given in section 5, and the discussion of results are contained in section 6. Finally, the main conclusions are listed in section 7.

2. Basic formulae

The double differential cross sections of weakly interacting magnetic systems is, to a good approximation, a sum of magnetic and nuclear parts

$$\frac{\mathrm{d}^2\sigma}{\mathrm{d}\Omega\,\mathrm{d}\omega} = \frac{\mathrm{d}^2\sigma_{\mathrm{nuc}}}{\mathrm{d}\Omega\,\mathrm{d}\omega} + \frac{\mathrm{d}^2\sigma_{\mathrm{m}}}{\mathrm{d}\Omega\,\mathrm{d}\omega}. \tag{1}$$

In what follows, the analysis of structure-related excitations will proceed along lines similar to those employed in a previous work [11], and therefore the reader is referred to the original paper for further details.

For a molecular system, no closed form is available to express the $S_{\mathrm{nuc}}(Q,\omega)$ dynamic structure factor without having to recourse to simplifying assumptions, in particular to the decoupling between centre of mass and rotational motions. On approximate grounds, assuming that such a coupling is effectively small, the nuclear scattering which gives rise to the double differential cross section can be written, for the case of a coherent scattering molecular unit as

$$\frac{\mathrm{d}^2\sigma_{\mathrm{nuc}}}{\mathrm{d}\Omega\,\mathrm{d}\omega} = \frac{|\boldsymbol{k}_0|}{|\boldsymbol{k}|} S_{\mathrm{nuc}}(Q,\omega) \tag{2}$$

$$S_{\mathrm{nuc}}(Q,\omega) = \frac{N}{2\pi} b_{\mathrm{O,coh}}^2 \int \mathrm{d}t \exp(-i\omega t) \left[\sum_{\mu,\nu} I_{\mu,\nu}(Q,t) I_s(Q,t) + F(Q)(I(Q,t) - I_s(Q,t))\right] \tag{3}$$

where $\boldsymbol{k}_0$ and $\boldsymbol{k}$ denote the incident and scattered neutron wavevectors respectively, $Q = \boldsymbol{k} - \boldsymbol{k}_0$, $\hbar\omega = \hbar^2/2m(k^2 - k_0^2)$. b_{O} denotes the coherent bound scattering amplitude for the oxygen nucleus and the sum over ν and μ runs over all the nuclei within the molecule. The intermediate scattering functions $I_s(Q,t)$, $I(Q,t)$ and $I_{\mu,\nu}(Q,t)$ are then given by

$$I_{\mu,\nu}(Q,t) = \langle \exp(\mathrm{i}\boldsymbol{Q}\cdot\boldsymbol{a}_\nu(t)) \exp(-\mathrm{i}\boldsymbol{Q}\cdot\boldsymbol{a}_\mu(0))\rangle \tag{4}$$

$$I_s(Q,t) = \frac{1}{N}\sum_i \langle \exp(\mathrm{i}\boldsymbol{Q}\cdot\boldsymbol{R}_i(t)) \exp(-\mathrm{i}\boldsymbol{Q}\cdot\boldsymbol{R}_i(0))\rangle \tag{5}$$

$$I(Q,t) = \frac{1}{N}\sum_{ij} \langle \exp(\mathrm{i}\boldsymbol{Q}\cdot\boldsymbol{R}_i(t)) \exp(-\mathrm{i}\boldsymbol{Q}\cdot\boldsymbol{R}_j(0))\rangle \tag{6}$$

and

$$F(Q) = \left(\sum_{\nu} \frac{\sin(Qa_{\nu})}{Qa_{\nu}} \right)^2 \tag{7}$$

where the angular bracket denotes an ensemble average and the sum over i and j runs over all the molecules in the system.

R_i is the position of the centre of mass (COM) and a_{ν} is the equilibrium position of the nucleus with respect to the COM

For a solid in which the molecules are fixed at the sites of a Bravais lattice, $I_s(Q,t) \simeq 1$ and therefore the equation given above becomes more simplified.

The intermediate scattering functions $I_s(Q,t)$ and $I(Q,t)$ may be accessed directly from the simulated trajectories. On the other hand the rotational functions $I_{\mu,\nu}(Q,t)$ are first expanded as

$$I_{\mu,\nu}(Q,t) = \sum_{l=0}^{\infty} (2l+1) j_l^2(Qa_O) P_l(\cos(\Theta_{\mu,\nu})) F_l(t) \tag{8}$$

and then calculated using the relation between the $F_l(t)$ and the autocorrelation function corresponding to the reorientation of a unit vector $u(t)$ pointing along some specified direction, i.e.

$$F_l(t) = \langle P_l(u \cdot u(t)) \rangle = \langle P_l(\cos\beta(t)) \rangle \tag{9}$$

where j_l, P_l and $F_l(t)$ are spherical Bessel functions, Legendre polynomials and rotational relaxation functions of order l respectively. The symbol $\Theta_{\mu,\nu}$ stands for the angle between atoms μ and ν which will take the values of π or 0 since we are dealing with a linear molecule, a_O is the distance from the oxygen nuclei to the COM and $\beta(t)$ is the angle through which a unit vector fixed in the molecule rotates in time t.

We recall that the magnetic scattering results from the interaction of the magnetic dipole moment of the neutron with the magnetic field produced by the unpaired electrons in the molecule and this field is determined by the total microscopic magnetization which arises from both the magnetic moment due to spins (nuclear and electronic) and to orbital motions. The resulting scattering law is related to the magnetic double differential cross section, which for a macroscopically paramagnetic system can be written as by [12]

$$(\mathrm{d}^2\sigma_{\mathrm{m}}/\mathrm{d}\Omega\,\mathrm{d}\omega) = (\gamma e^2/m_e c^2)^2 (k/k_0) |\tfrac{1}{2} g f(Q)|^2 S_{\mathrm{m}}(Q,\omega) \tag{10}$$

where $(\gamma e^2/m_e c^2)^2 = 0.291$ barn is the coupling constant of the neutron and the magnetic system, $g = 2$ is the Landé factor for systems with quenched orbital momentum such as the one we are dealing with, and $f(Q)$ is the molecular magnetic form factor which was taken from [13].

The relationship between the scattering law and the spin dynamics is encompassed by [12],

$$S_{\mathrm{m}}(Q,\omega) = \frac{1}{2\pi} \int \mathrm{d}t \exp(-\mathrm{i}\omega t) \sum_{ij} \exp[\mathrm{i}(Q(r_i - r_j))] \langle S_i(t) \cdot S_j(0) \rangle \tag{11}$$

where the spin correlation function contains all the sought information regarding the dynamics, and the summation runs over different spins. For paramagnets all the scattering is inelastic and the scattering law is commonly defined through the $F(Q,\omega)$ spectral weight function,

$$S_m(Q,\omega) = (n(\omega)+1)\chi''(Q,\omega) = \omega[n(\omega)+1]\chi_Q F(Q,\omega) \qquad (12)$$

where the $(n(\omega)+1)$ factor accounts for detailed balancing, $\chi''(Q,\omega)$ is the imaginary part of the dynamical susceptibility and χ_Q represents the static, wavevector-dependent susceptibility (the frequency integral of the dynamic susceptibility times $1/\omega$).

3. Molecular dynamics calculations and experimental details

Following the previous work on lattice dynamics of the low-temperature- ordered α and β solid phase and that done on the γ phase [14,15], we use a site–site Lennard-Jones intermolecular potential

$$U(\boldsymbol{R}_{12},\omega_1,\omega_2) = \sum_{\alpha,\beta} U_{\alpha,\beta}(r_{\alpha,\beta}) \qquad (13)$$

where $\boldsymbol{R}_{12}$ is the vector joining the centre of molecule 1 to that of molecule 2, ω_i is the orientation of molecule i, $r_{\alpha,\beta}$ is the distance between site α on molecule 1 and site β on molecule 2, and

$$U_{\alpha,\beta}(r_{\alpha,\beta}) = 4\epsilon_{\alpha,\beta}[(\sigma_{\alpha,\beta}/r)^{12} - (\sigma_{\alpha,\beta}/r)^6]. \qquad (14)$$

Three runs corresponding to the solid γ phase at 50 K and to the liquid phases at 55 K and 88 K have been carried out. The relevant potential parameters correspond to those of ref [16]. Both translational and rotational equations of motion have been solved by applying the Gear predictor–corrector method [17]. The COM motions of the molecules were followed using a fifth-order algorithm. The Euler's equations of motion in quaternions were solved by a fourth-order algorithm. The molecules were confined in a cubic box of length L (27.03 Å for $T = 50$ K, 21.84 Å for $T = 55$ and 22.74 Å for $T = 88$ K) and subjected to periodic boundary conditions. The number of molecules (256 molecules for the liquid and 512 for the γ phase) and the volume of the box were chosen to give the number density of the physical system under study. The corresponding molar volumes were 23.22 cm^3 for the solid and 24.5 cm^3 and 27.67 cm^3 for the liquid. The chosen time step was of 0.02 ps and the simulations were run for a total of 30 ps (after equilibration) The boundary conditions have the consequence that when a particle leaves the box through one side, its image enters through the opposite side thus preserving the number of particles in the box. These conditions eliminate strong surface effects and in some respects, simulate an infinite system.

The neutron experiments were performed using the IN6 spectrometer located at the Institut Laue–Langevin (ILL, Grenoble, France). The measurements were carried out at 35 K and 50 K in the solid phase and at 55 K and 88 K in the liquid phase using an incident wavelength of 4.1 Å, corresponding to a resolution in energy transfers (full width at half maximum) of about 0.17 meV. The sample container was a cylinder of 10 cm^3 capacity, which allows the in-cell condensation of room temperature O_2 gas from a pressure vessel directly inside the helium cryostat.

The spectra were then corrected by standard ILL programs for detector efficiency, sample container, absorption and self-shielding. The number of multiply scattered neutrons was reduced to a minimum by inserting five cadmium spacers of thickness 0.1 mm and then was estimated using the DISCUS code [18] and was subtracted from the measured total intensities. The dynamical structure factor $S(Q,\omega)$ were then converted into constant Q with the INGRID code [19]. In order to match the same set of momentum-transfer values accessed by the simulation, the constant-Q spectra were generated for the same set of wavevectors using such an interpolation scheme. A set of spectra for the solid γ and the liquid phases, showing the structural and the magnetic contributions is shown in figure 8.

Because of the complications of estimating a total density of states from the measured spectra, since there seems to be no theoretical recipe available [20], the quantities

$$J(Q,\omega) = (\omega^2/Q^2)S(Q,\omega) \tag{15}$$

which are related to longitudinal current density and spin fluctuactions, were also calculated for selected momentum transfers.

4. Molecular dynamics results

From the molecular dynamics data which are the generated positions, linear and angular velocities, and quaternions, the following functions have been calculated by means of formulae which are given in a previous paper [11].

4.1. Radial distribution function $g(r)$

The relevant information on the short-range structure is contained in the radial distribution function $g(r)$. This function calculated for the molecular centres of mass is shown in figure 1 for both the solid γ and the liquid phases. This figure shows that the most probable distribution of the molecule COM is around 3.7 Å for both the solid and the liquid. This position coincides with that reported in [21] from an unpolarized neutron diffraction experiment. The amplitude at the first minimum (around 5 Å) for the solid phase is approximately zero indicating that there is no molecule around the position of this minimum while in the liquid the amplitude of this minimum is different from zero. The second maximum in $g(r)$ which indicates the second most probable distance is split into two peaks in the solid. The numbers of first and second neighbours are given by 2.77 and 2.01 for the solid, 2.76 and 3.12 for the liquid at 55 K and 2.86 and 3.28 for the liquid at 88 K. The first neighbours in the solid γ phase are those molecules separated by a distance $a/2$ and $a\sqrt{5}/4$ where a is the length of the unit cell ($a = 6.7565$ Å).

From the analysis of the mean square displacements calculated for the two temperatures in the liquid phase as well as for the γ phase, it was found that the equilibrium was reached after about 2 ps following, in the case of the liquid, a linear behaviour with time and an oscillation of $\langle r^2(t)\rangle$ around a constant value for the solid. The values for the self-diffusion coefficient of 0.39×10^{-5} cm^2 s^{-1} and 2.41×10^{-5} cm^2 s^{-1} for $T = 55$ K and 88 K respectively were computed from the slope of the curves corresponding to the liquid phase, and are in good agreement with the ones estimated from corresponding state arguments [9]. At times much shorter than the characteristic collision time, any tagged molecule is expected to move freely

and hence its mean square displacement is given by $v_0^2 t^2$ where v_0 is the thermal velocity. From plots of this quantity versus time for the liquid phases it was found that the free movement lasts only 0.2 ps.

4.2. Velocity autocorrelation functions

The total velocity of an oxygen atom v_O within the molecule can be expressed in terms of the COM and angular velocities as [22]

$$v_O = v_{COM} + \omega \times a_\nu \tag{16}$$

where the first term accounts for the translational motion, ω is the angular velocity and a_ν is the nuclear displacement vector, which specifies the atomic position with respect to the COM The dynamics of the total, centre-of-mass and reorientational motions can be best described in terms of the velocity autocorrelation functions for the total, COM, and angular velocities, as well as coupling terms which account for the interaction between translation and rotation at a microscopic scale.

The relevant functions are displayed in figure 2 for the three studied temperatures. The binary collisions (short-time) region in the atomic (and COM) velocity autocorrelations lasts for about 0.3 ps in all the phases. On the other hand, the broad backscattering region lasts for relatively long times (above 1.5 ps) and clear oscillations within this range become more pronounced as the temperature is decreased. The period of such an oscillation (roughly 3.3 ps) will result in a noticeable structure in the Fourier spectrum of such autocorrelations (proportional to the generalized frequency distributions) which, as shown in figure 3, will show noticeable departures from the simple Brownian behaviour.

The estimates for the self-diffusion coefficient can also be obtained from the time integral of these functions, and therefore they provide a consistency check between the result calculated from the mean square displacement and the integral of the COM velocity autocorrelations. The diffusion coefficients calculated by this means from the integral of the COM functions are equal to 0.45×10^{-5} cm^2 s^{-1} and 2.49×10^{-5} cm^2 s^{-1} for $T = 55$ K and 88 K respectively and are indeed consistent with the ones deduced before.

The normalized angular velocity autocorrelations (AVACF) are also shown in figure 2 for the three runs. From this figure we see that the AVACF for the liquid at 55 K and the solid γ phase have the same behaviour for times less than 0.4 ps suggesting that for short times the same processes occur in these two phases. As was evidenced for the VACF a less pronounced minimum appears for the liquid at 55 K than the solid which is an indication of the reverse rotation caused by the impact with the neighbouring molecules. At 88 K the AVACF does not show any negative minimum which indicates the difficulty in reversing the direction of the rotational excursions by means of collisions with the cage of its neighbours. At this temperature, both the linear and angular velocity correlation functions become remarkably similar in shape. A reorientational correlation time τ_ω can be defined as:

$$\tau_\omega = \frac{\int \langle \omega(0)\omega(t) \rangle \, dt}{\langle \omega^2(0) \rangle} \tag{17}$$

and is equal to 0.137 ps, 0.129 ps and 0.216 ps for 50, 55 and 88 K respectively.

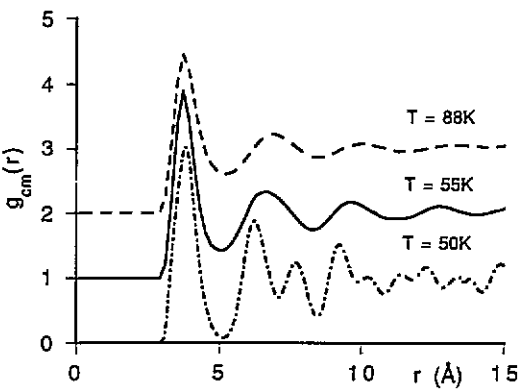

Figure 1. Static $g(r)$ pair correlation functions for the molecular COM. The functions correspond (from bottom to top) to the plastic-crystalline solid, liquid near melting and boiling points respectively.

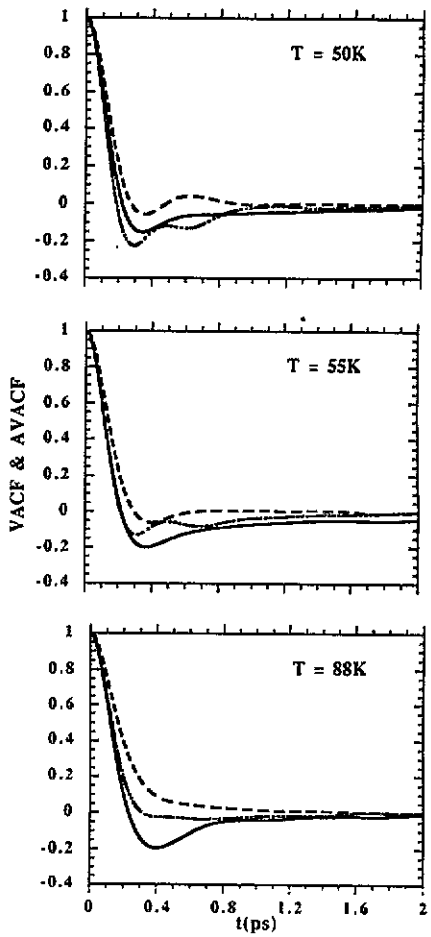

Figure 2. Velocity autocorrelation functions. (——) represents the autocorrelation for the total atomic velocity, (— · —) the COM function and (- - -) shows the angular velocity autocorrelation.

4.3. Rotational relaxation functions

The rotational relaxation functions $F_1(t)$ and $F_2(t)$ are presented in figure 4 as well as their fit with an exponential function and a function used by Levesque [23]. If we assume that molecular orientation takes place by means of a rotational random-walk process i.e. a rotational diffusion model, the relaxation function $F_l(t)$ should have an exponential decay following:

$$F_l(t) = \exp(-l(l+1)D_r t) \tag{18}$$

where the rotational correlation time τ_l required so that a substantial reorientation of the molecules take place is given by: $\tau_l = (l(l+1)D_r)^{-1}$ where D_r is the rotational diffusion constant. The relaxation functions $F_1(t)$ may be reproduced by an exponential function and give rotational diffusion constants of about 0.58, 0.54 and 1.16 ps^{-1} for the three temperatures 50, 55 and 88 K respectively. On the other hand

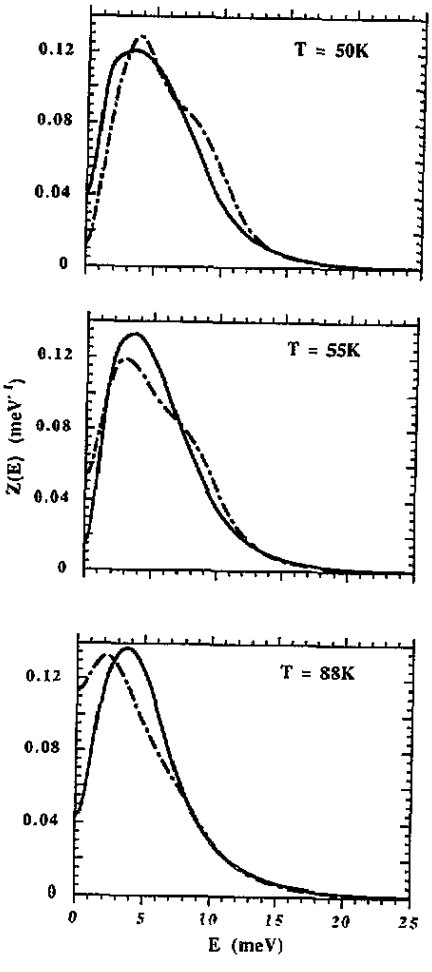

Figure 3. Frequency spectra of the velocity autocorrelation functions. (——) shows the total $Z(E)$ densities of states (i.e. the transform of the total atomic velocity), and (— · —) shows the COM spectra.

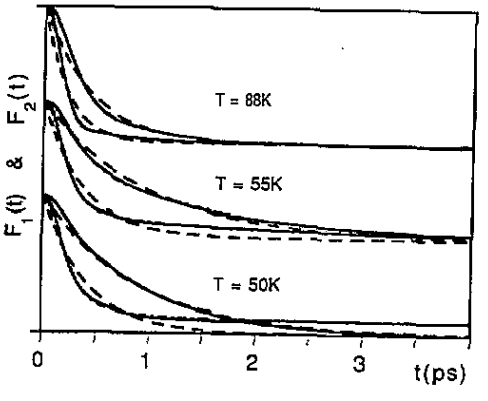

Figure 4. Rotational relaxation functions (——) for γ and liquid phases. (– – –) represents the best approximation attainable using an exponential (rotational diffusion) model. (— · —), very close to the computer-simulated functions, are the approximation using the empirical function due to Levesque [23] (see text).

the correlation functions $F_2(t)$ give poor fits to an exponential function and thus the rotational diffusion model is only very approximately valid in the case of molecular oxygen. As for the AVACF we can define the correlation time τ_l by:

$$\tau_l = \int F_l(t)\,\mathrm{d}t \tag{19}$$

and the correlation times τ_1 and τ_2 corresponding to the three studied temperatures were found to be $\tau_1 = 0.80$ ps, 0.97 ps and 0.42 ps for $T = 50$ K, 55 K and 88 K, and $\tau_2 = 0.99$ ps, 0.54 ps and 0.24 ps for the same values of the temperature. In order to avoid problems of evaluation of this integral at long times, the integral has been

calculated for the function used by Levesque which best reproduces the relaxation functions at all studied temperatures.

4.4. Rotational dynamics in the solid phase

As we have mentioned before, in the solid γ phase, two molecules from the eight existing in the unit cell are assumed to execute reorientational motions isotropically (spherically), whereas the remaining six are confined to rotate within a plane. In order to check this assumption, we have calculated separately for each kind of molecule and over all the molecules in a configuration the average value of the x, y and z component of the unit vector defined by each molecule. The obtained results show that molecules of kinds 1 and 2 have the same (non-zero) average for the three orthogonal directions of the unit cell which is an indication of orientational isotropy, whereas molecules of types 3 and 4 have a vanishing average for the y component, thus indicating their confinement to the x–z plane. On the other hand, molecules of types 5 and 6 as well as 7 and 8 show an equivalent behaviour, being in these latter cases confined to the x–y and y–z respectively.

We have also computed the average values for the angle θ_1 defined by the internuclear vector of a molecule and the axis joining this molecule with another contained in the same unit cell, (i.e. the angle between molecule 3 and the 3–4 axis). This angle was found to fluctuate around an average value of 90° ($84 \leqslant \theta_1 \leqslant 96$), thus confirming the picture which describes the disk-shaped molecules as rotating within parallel disks.

Another relevant geometrical quantity is constituted by the average angle θ_2 defined by the vectors along the internuclear axes of neighbouring molecules. An average value of 48.7° was found, and the angular excursions were found to be confined within the range of ($46 \leqslant \theta_2 \leqslant 52$). The H model of Cox *et al* [4] which consists of a translation–rotation correlation and which best fits the structure gives an angle equal to 45° (the fits remain good in the range 20–70°) [4, 7].

From consideration of the results given above, it seems clear that the rotational dynamics of the two different kinds of molecules require two relaxation times for its description. As expected, the fits to the $F_1(t)$ and $F_2(t)$ greatly improve after allowance is made for these different processes, and the same phenomena seems to occur in the liquid phase.

4.5. Total dynamical structure factor

The correlation function $I(Q,t)$ is shown in figure 5 for the liquid and the solid phases at the lowest values of Q accessible to our simulation; where finite-frequency excitations are clearly visible. Bezugly [24] deduced the isothermal compressibility from values of the isothermal velocities and obtained a value of 6.06×10^{-10} m^2 N^{-1} for $T = 50$ K. In the limit of small Q, $S(0)$ which is equal to $I(0,0)$ is given by:

$$S(0) = \rho_0 \chi_T k_B T \tag{20}$$

where ρ_0 is the density. The value obtained for S(0) (0.0108) can be compared with the one calculated for the lowest Q-value accessible in this simulation, which gives 0.0078.

The dynamical structure factor calculated from the analysis of the computed trajectories by means of (3) is shown in figure 5 for the liquid and solid phases for the lowest momentum transfer accessible to the simulation. From comparison

between the polycrystalline $S_{nuc}(Q,\omega)$ and those of the liquid phase, the observed excitation in the liquid can be assigned to a sound mode. The derived values of the sound velocity 1241 m s^{-1} at 55 K and 797 m s^{-1} at 88 K are in reasonable agreement with those measured in the hydrodynamic limit 1195 m s^{-1} and 920 m s^{-1} for $T = 55$ and 88 K respectively [25]. For 50 K the value derived for the sound velocity 1516 m s^{-1} is comparable to the one given by Klein [8] (1600 m s^{-1}).

As was mentioned above, the rotational disorder present in the plastic-crystal phase substantially broadens the observed response function making its lineshape and linewidth rather similar to that of the cold liquid, with exception being made of the low-frequency peak which is enhanced in the liquid due to the contribution of diffusional effects to the quasi-elastic response. In contrast, the COM functions which were also calculated for the polycrystal evidenced the presence of a rather structured response.

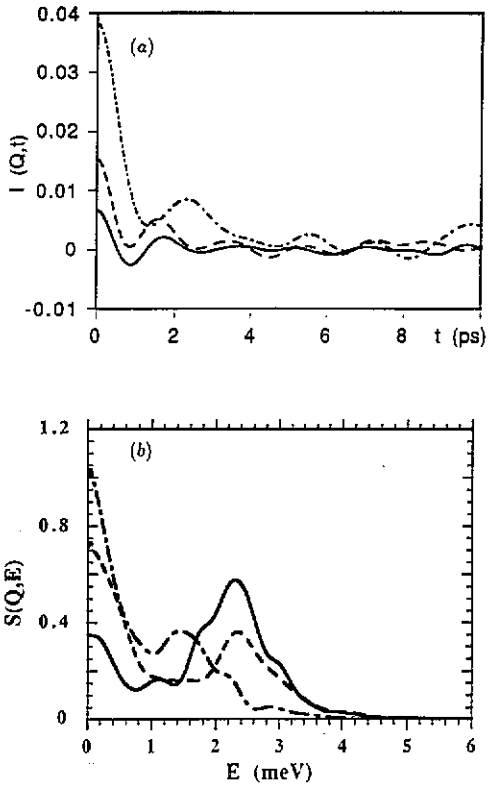

Figure 5. (*a*) shows the $I(Q,t)$ intermediate scattering functions, and (*b*) displays a comparison between the calculated $S_{nuc}(Q,\omega)$ dynamic structure factors for the plastic crystal (solid) and the liquid at the two temperatures explored, $T = 55$ K (– – –) and $T = 88$ K (— · —). The spectra correspond to a momentum-transfer value of $Q = 0.28$ Å^{-1} for the liquid phase and $Q = 0.23$ Å^{-1} for the solid.

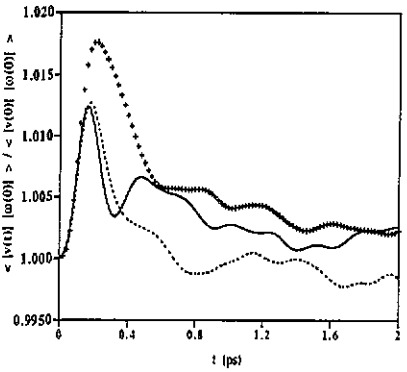

Figure 6. Linear/angular speed autocorrelation functions. (——) shows the result for the plastic crystal, (· · · · · ·) the low-temperature liquid and (+) plot this function for the high-temperature liquid.

Finally, and in order to assess the amount of coupling between molecular rotations

and COM motions, we have calculated the first non-vanishing mixed autocorrelation function, i.e. $\langle|v_{COM}(t)||\omega|(0)\rangle/\langle|v_{COM}(0)||\omega|(0)\rangle$, and the results for the three studied temperatures are shown in figure 6. As can be easily seen from inspection of the graph, the three thermodynamic states behave in rather different ways. Below 0.4 ps the coupling is very similar for the plastic-crystal and cold-liquid phases, but becomes more marked for the high temperature liquid. On the other hand, the solid, as expected, exhibits a more marked oscillatory behaviour than the liquid.

5. Experimental results

The broad quasi-elastic component which is seen in the experimental spectra can be considered to be a clear signature of a magnetic effect. Otherwise, the magnitude of the relevant transport coefficients derived from such a broadening (self-diffusion or rotational), would have to be at least one order of magnitude larger than the value obtained from other experimental means.

In order to assess the relative importance of the magnetic response, the $J(Q,\omega)$ functions calculated for some selected values of momentum transfer are displayed in figure 7 for temperatures corresponding to the short-range magnetically ordered β phase at 35 K, where the rotational contributions should not give rise to important quasi-elastic scattering, as well as for the γ phase (50 K) and for the two temperatures corresponding to the liquid range (55 K and 88 K). The chosen values for Q correspond to a region about the maxima of the magnetic structure factor ($Q = 1.4$ Å^{-1}) [7] and a region ($Q = 2.2$ Å^{-1}) where the intensity of magnetic origin is considerably reduced.

As can be seen from the figure, the shape and amplitude of these functions for the plastic crystal and the cold liquid are strikingly similar, showing a broad maximum at about 4.5 meV. The main differences between the plastic-crystal and the orientationally ordered β phase are the smaller amplitude of the curve corresponding to the latter phase as well as the low-frequency tail which displays a larger concavity. Also, the spectrum of the hot liquid shows a larger intensity, something which can be explained if the large difference in the reorientational parameters for the plastic crystal (or cold liquid) and those corresponding to this thermodynamic state are taken into account [26].

On the other hand, the curves corresponding to $Q = 2.2$ Å^{-1} (i.e. well above the maxima of the magnetic and liquid-structure peaks) show that the maxima of the plastic-crystal and liquid peaks are located at a somewhat lower energy than that corresponding to the β phase (3.5 meV vs $\simeq$ 4 meV). Also, the main differences between the plastic and cold-liquid phases are located in the low-frequency tails, and the difference in intensity regarding the high-temperature liquid can also be understood following the same arguments outlined above [26].

As a consequence, most of the spectral power giving rise to finite-frequency features in the $J(Q,\omega)$ functions arises from magnetic fluctuactions, and those of structural origin contribute as a featureless background, with a height and width which increases with temperature.

The spectra were analysed in terms of the following $S(Q,\omega)$ model scattering law

$$S_{mod}(Q,\omega) = a(S_{nuc}(Q,\omega) + S_m(Q,\omega)) \tag{21}$$

where a is a global scaling factor and $S_{nuc}(Q,\omega)$ is obtained from the simulation. The magnetic contribution $S_m(Q,\omega)$ was assumed to have a lineshape characteristic

of a Heisenberg paramagnet [27,28], which has proved to be a reliable tool for data analysis purposes on a number of metallic or insulating paramagnets [29]

$$S_m(Q,\omega) = \omega/[1-\exp(-\omega/k_BT)]\chi_Q F(Q,\omega) \tag{22}$$

$$F(Q,\omega) = \tau\omega_0^2(\omega_s^2-\omega_0^2)/\pi\{([\tau\omega(\omega^2-\omega_s^2)]^2+(\omega^2-\omega_0^2)^2)\} \tag{23}$$

where χ_Q is the static susceptibility, $F(Q,\omega)$ the spectral weight function, integrals of which times ω^2 and ω^4 generate relationships between the spectral moments. The parameter τ is a relaxation time and ω_0^2 and ω_s^2 are related to the second and fourth frequency moments of the spectral weight function throughout

$$\langle\omega^2\rangle = \omega_0^2 \tag{24}$$

$$\langle\omega^4\rangle = \omega_0^2\omega_s^2 \tag{25}$$

and the relaxation time was evaluated using the prescription [28]

$$\tau^{-1} = [\pi(\omega_s^2-\omega_0^2)]^{1/2}. \tag{26}$$

A set of spectra showing all these contributions is presented in figure 8. The second and fourth moments extracted in this way are presented in figure 9 for temperatures corresponding to the plastic crystal and cold liquid.

In a previous work [10], an attempt was made to interpret the wavevector dependence of the second frequency moment by means of a simplified adaptation of a model for linear exchange-coupled paramagnets, where only nearest-neighbour interactions were taken into account.

Leaving the value of the exchange constant and the distance to the first neighbours as adjustable parameters, it was found that the second moment was qualitatively reproduced when the coupling was assumed to be of ferromagnetic nature. The values obtained for both parameters were $J = 22$ K and $d = 2.9$ Å, which, although being in reasonable agreement with those estimated from polarized neutron diffraction, predicted a sign for the exchange constant opposite to what was observed in diffraction experiments.

In order to reconcile such an apparent discrepancy, we have tried to model the spectral moments following two different approaches. The first one uses a result from coupled-mode theory as developed in [30], and assumes interactions between nearest neighbours only in one dimension. Leaving aside the case of the liquid phase, where a calculation applicable to a one-dimensional magnetic material cannot be taken too far, we have tried to estimate some values for the exchange-coupling constant as well as for the distance to the nearest neighbour, for the plastic-crystal for which a quasi-one-dimensional nature has been postulated [31]. The formulae for the second and fourth frequency moments of the spectral weight function have been adapted using a polycrystalline average of those developed from a refined version of the coupled-mode theory [30]

$$\omega_0^2 = 4Ju(1-j_0(Qd))/3\chi_Q \tag{27}$$

$$\omega_s^2 = (2J^3/3)\{5-3j_0(Qd)+v(1-3j_0(Qd)+3/u) - u[6j_0(Qd)-(2+v)(2j_0^2(Qd)-1)]\} \tag{28}$$

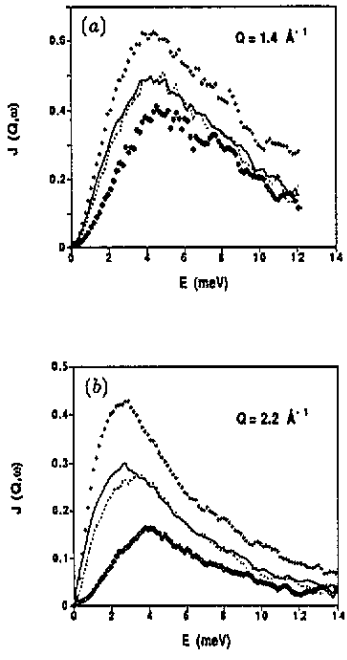

Figure 7. Longitudinal current correlation functions $J(Q,\omega)$. (*a*) shows the functions calculated for $Q = 1.4$ Å^{-1} for $T = 35$ K (◇), $T = 50$ K (·····), $T = 55$ K (——) and $T = 88$ K (+). (*b*) displays the functions for $Q = 2.2$ Å^{-1} (same symbols are used).

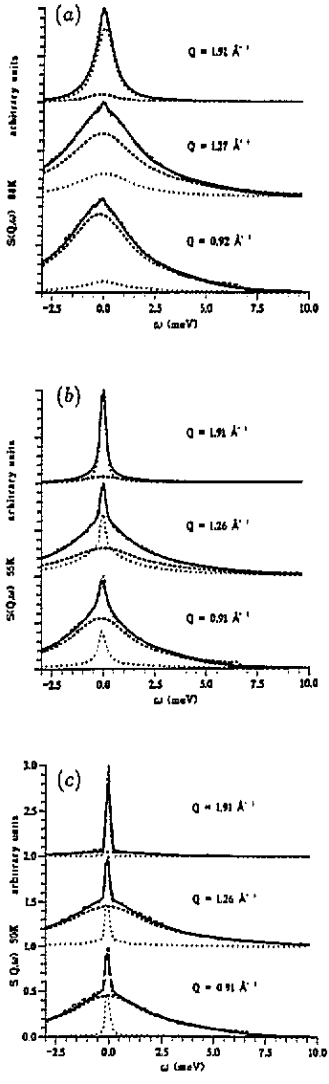

Figure 8. A set of spectra for (*a*) liquid, (*b*) cold liquid and (*c*) plastic-crystal close to boiling illustrating the structural (·····) and magnetic (– – –) contributions to the total (— · — which is only visible in some spectra) inelastic intensities. (——) represents the fitted model.

with $u = \coth(J/T) - T/J$ and $v = 1 - 3uT/J$. j_0 is a spherical Bessel function, and the static susceptibility is given by

$$\chi_Q = (1-u^2)/\{3T[1+u^2-2uj_0(Qd)]\}. \tag{29}$$

A comparison between the moments derived from the analysis of the lineshape for the plastic crystal and those calculated using such an approach taking for the exchange constant and the nearest-neighbour distance the values derived from

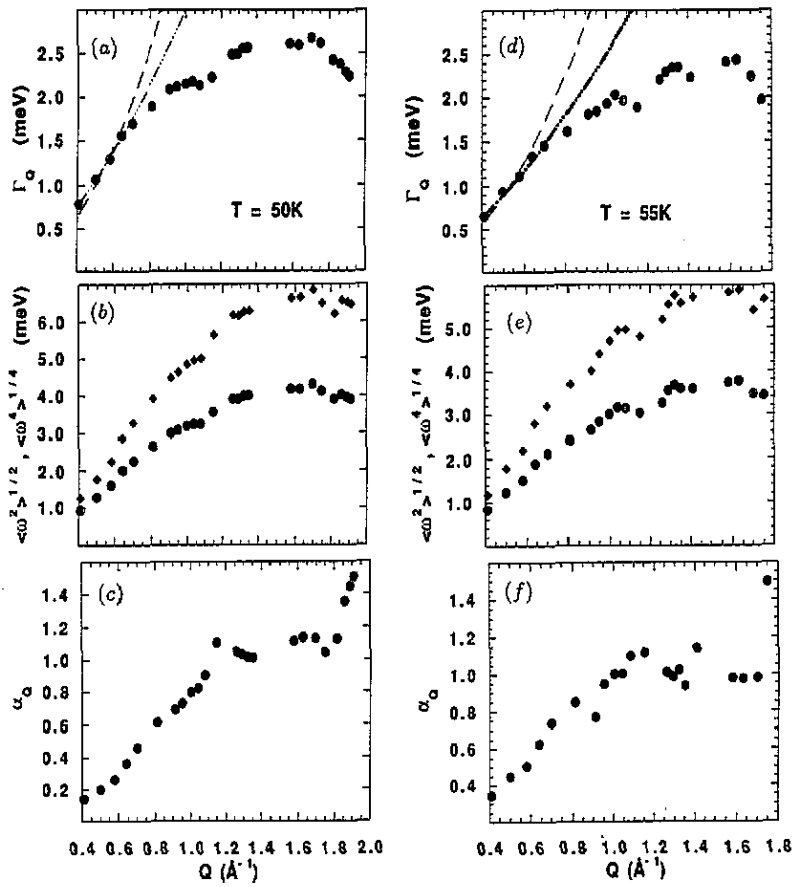

Figure 9. Spectral parameters for the γ ($T = 50$ K) and cold liquid ($T = 55$ K) phases. (*a*) and (*d*) show the linewidths as computed from (31) (●) and the hydrodynamic approximations which follow a Q^2-dependence (– – –) and a $Q^{3/2}$-dependence (— · —). (*b*) and (*e*) show the reduced second (●) and fourth (♦) frequency moments. (*c*) and (*f*) show the lineshape parameter α_Q, as calculated from (32).

polarized diffraction experiment is shown in figure 10, and further discussion is deferred to the next section.

In order to analyse the frequency moments corresponding to the liquid data, we have computed the values of ω_0^2 by means of a slight generalization of the expression for the f sum rule given in a number of papers [12,32] for a Heisenberg model at infinite temperature,

$$\omega_0^2 = \tfrac{8}{3}S(S+1)\int_0^\infty \mathrm{d}r J^2(r)g(r)r^2(1-j_0(Qr)) \tag{30}$$

where the values for the distance-dependent exchange coupling were taken from estimates given in [33,34], and $g(r)$ is the pair correlation function for which the magnitude referred to the distribution of molecular centres of mass was taken. The results of such a computation with those derived from experimental means are shown

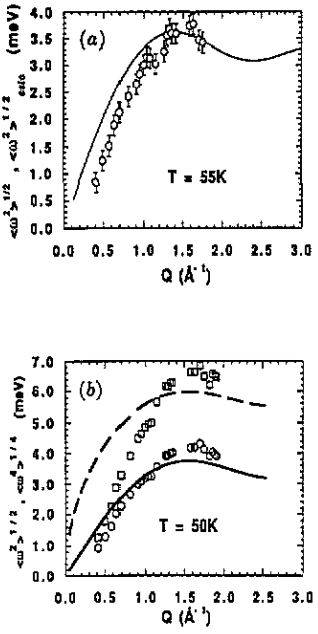

Figure 10. (*a*) shows a comparison between the reduced second moment as calculated from (30) (——) and experimental (O). (*b*) displays a comparison between the second (——) and fourth (– – –) frequency moments as calculated using equations (27)–(28) with those derived from experimental measurements (O and □).

in figure 10, for which only a global scale parameter was used since no other adjustable constant enters in this comparison.

In order to compare the obtained results on a model-free basis we have also calculated the spectral linewidth from the ratio of the the frequency moments as [12,27,28],

$$\Gamma_Q = (\pi/2)[\langle\omega^2\rangle^3/\langle\omega^4\rangle]^{1/2} \tag{31}$$

where it is implicitly assumed that at low momentum transfers, the spectral function approaches a Lorentzian form. The results for two temperatures corresponding to the γ and cold-liquid phases are shown if figure 9 along with a comparison with the hydrodynamic behaviour and with that predicted by the dynamic scaling hypothesis. The low-Q region shows a behaviour which seems closer to the $D_sQ^{3/2}$ law which characterizes an antiferromagnetic coupling mechanism, than to a D_sQ^2, relevant for simple diffusion. In both cases, D_s is interpreted as a spin diffusion coefficient, and the corresponding values for both kinds of behaviour were of $D_s = 4.0$ meV Å^2, $D_s = 3.8$ meV Å^2 and $D_s = 3.5$ meV Å^2 for $T = 50$ K, 55 K and 88 K for normal diffusion and $D_s = 3.1$ meV Å$^{3/2}$, $D_s = 2.9$ meV Å$^{3/2}$ and $D_s = 2.6$ meV Å$^{3/2}$ for the same temperatures for the $D_sQ^{3/2}$ law respectively. It becomes difficult to verify such a behaviour due to the number of approximations involved for its derivation (i.e. the procedure to separate the magnetic contribution and the calculation of the linewidth on a hydrodynamical basis).

6. Discussion

The conditions for the validity of the separation between the structural and magnetic responses as sketched in the introduction, have been shown to be fulfilled after

the computation of the relevant transport coefficients from the analysis of the MD trajectories.

Even if the cross section for unpolarized neutrons appears, at some wavevectors and energy transfers, to be dominated by the magnetic response, the thermodynamical properties of both γ and liquid oxygen do not seem to encompass large contributions of magnetic origin. As a matter of fact, an estimate of the specific heat using the total densities of states computed from the simulations gives values of 42.1, 43.3 and 46.8 J $K^{-1}mol^{-1}$ for $T = 50$ K, 55 K and 88 K respectively, which gives differences of 4.8, 11.0 and 10.7 J $K^{-1}mol^{-1}$ with the experimental total heat capacity which includes a magnetic contribution which presumably will be small [36]. The differences quoted above can therefore be used to give an upper bound to such a contribution to the specific heat, a property which is in this case hardly amenable to experimental measurement.

A remarkable similarity, as far as the atomic dynamics is concerned, between the plastic-crystal and liquid phases has been evidenced. In particular the velocity autocorrelation functions involving both the total velocity and the reorientational motion have been shown to exhibit a similar behaviour in the cold-liquid and γ phase for short times (up to 0.4 ps), thus giving further support to the hypothesis of parallel arrangements taking place in the liquid for short times [21]. On the other hand, the moderate amount of rotation–translation coupling found even in the solid phase, can be understood if one considers similar cases studied in more detail regarding this particular aspect, such as condensed nitrogen [37].

Disordered molecular oxygen has been portrayed as a quasi-one-dimensional magnetic material [31], from consideration of the large differences between the exchange couplings between molecules rotating within parallel disks (DD), between disks and spheres (DS) and between spheres (SS) themselves. As a matter of fact, values of the order of $J_{DD} = 25$ K, $J_{DS} = 0.2$ K and $J_{SS} = 0.05$ K, were found to be necessary to reproduce the susceptibility data [5]. From the analysis of the polarized neutron diffraction cross sections [7], the presence of strong antiferromagnetic correlations between disks was inferred for the plastic-crystal, and also, from the similarity of spectra between the liquid and plastic-crystal phases, the existence of the same type of correlations within the liquid phase was postulated, at least for short times. The interactions between next-nearest disks were also found to be very weak by Dunstetter *et al* [7] and also the interactions between spheres and disks was found to be negligible for profile refinement purposes. The data presented here gives further support to such an interpretation since the main features regarding the spectral moments characterizing the magnetic dynamics can be qualitatively reproduced by means of simplified one-dimensional Heisenberg models. As is evident from inspection of figure 10, the larger deviations between the simplified model and experimental data concern the shape of the reduced fourth frequency moment, something which could be expected since four-spin correlation functions will contribute significantly to the spectrum and are not easily modelled.

Under the experimental conditions where the measurement was performed, it is clear that the observed magnetic response is diffusive in nature. To this respect, it is worth emphasizing the fact that because of the low incident energy employed in the present set of measurements, a very restricted kinematical range was available (the useful dynamic range was confined between $0.6\ \text{Å}^{-1} \leqslant Q \leqslant 1.8\ \text{Å}^{-1}$). On the other hand, the region about the Brillouin zone boundary was then left mainly unexplored since, no finite-frequency features were expected to appear in the energy-gain side of

the spectra at this, relatively low temperature (50 K). In this respect it is worth noting that even for a classical Heisenberg-spin chain at infinite temperature, the existence of finite-frequency excitations which manifest themselves as broad flat-top curves (square spectra) has been postulated from simulation results [35]. An assessment of the existence of a finite-frequency excitation can be made if negative values are found for the parameter

$$\alpha_Q = \tfrac{1}{3}((\omega_s^2 - \omega_0^2)/\omega_0^2 - 2). \tag{32}$$

The range of values found from the computed moments for the γ and liquid phases is shown in figure 9, where positive values were found for all the explored wavevectors thus indicating the diffusive nature of the magnetic response.

A recent muon spin-rotation (μSR) study [38] has revealed that, a strong variation in the depolarization ratio occured within the temperature range corresponding to the solid β and γ phases, showing a strong peak in the vicinity of the β–γ transition. To explain such a phenomenon, the interaction of the muons with the rotational magnetic moment of the oxygen molecule was adduced. However, the close similarity found for the rotational dynamics of the γ and cold-liquid phases (no substantial variation in the muon relaxation rate was found for all the liquid range), seems to invalidate such an explanation. Further μSR measurements on a longitudinal field may throw some light on this discrepancy.

7. Conclusions

The magnetic correlations which are present in the spectral response on a molecular paramagnet have been shown to be of dynamic origin.

Even if the separation between the structural and magnetic parts of the total spectra is of an approximate nature, the consistency checks made in order to attest the reliability of the MD simulation and to demonstrate that the present analysis is consistent with the findings of polarized neutron diffraction, provide a way to assert the physical soundness of the obtained results. Furthermore, the large differences (more than one order of magnitude) between the transport coefficients of structural origin (self-diffusion and rotation) and those related to the spins (D_s) have enabled such a separation to be made on a safe basis.

At the present level of refinement (i.e. the exchange couplings are assumed to be dependent on the internuclear distance only) the comparisons between experimental and calculated magnitudes have to be performed on a semiquantitative basis.

From what is known from *ab initio* quantum chemical calculations for pairs of oxygen molecules [39], the value of the exchange coupling constant shows a strong dependence on the interparticle separation as well as on the relative molecular orientation. It is then of no surprise that the agreement between calculated and experimental spectral moments is only qualitative, since a full knowledge of the function $J(r,\Omega)$, where Ω represents the Euler angles specifying the relative position of one molecule with respect to an axis fixed on the other, is needed. On the other hand, the parametric formulae such as the one employed in the present comparison, have been shown to be correct for a limited range of distances only [33]. Therefore, this work calls for first-principles MD simulations to be made on this material since studies performed using a relatively small number of particles can provide very valuable information regarding the coupling mechanism. Also, spin

dynamics simulations of the kind of those described by Gerling *et al* [35], may prove to be of great value in providing a mapping of the kinematical region where finite-frequency excitations, if they exist, can be located.

The distance dependence of the exchange coupling constants as well as the magnetic correlation lengths, do not seem to be very different, in the γ or liquid phases, to those of the two-dimensional magnetically short-range ordered β phase. As a matter of fact, the spectral moments are qualitatively reproduced using the tabulated function values for $J(r)$, and, as shown in a previous communication, the correlation length cannot exceed 5.2 Å [9].

From the point of view of the atomic dynamics, the present study has corroborated the existence of strong correlations between unit vectors along the internuclear axis of neighbouring, disk-shaped molecules. The presence of such a strong coupling of relative orientations was postulated from the analysis of the diffraction intensities in the plastic-crystal phase [40], and the present study has revealed the structural origin (i.e. generated by the force field of neighbouring molecules) of such a phenomenon.

Acknowledgments

Work supported in part by DGICYT grant (Spain) No PB89-0037-C03. Dr A J Dianoux from the Institut Laue–Langevin is kindly thanked for the help given during the performance of the experimental measurements. Very helpful discussions with Dr F Dunstetter from the Laboratoire des Solides Irradiés, Ecole Polytechnique, Palaiseau (Paris) regarding structural phenomena taking place in the solid phase are warmly acknowledged. Dr R J Meier from DSM-Research (The Netherlands) is also thanked for his help in making available to us a copy of his PhD dissertation.

References

[1] Kammerlingh-Onnes H and Perrier A 1910 *Comm. Phys. Lab. Leiden* **116** 1
[2] Alikhanov R A, Vul E B and Federov J G 1967 *Acta Crystallogr.* **A92** 21
Barret C S and Meyer L 1967 *Phys. Rev.* **160** 694
Alikhanov R A 1967 *JETP Lett.* **5** 349
[3] Horl E M 1962 *Acta Crystallogr.* **15** 845
Alikhanov R A 1964 *Sov. Phys. JETP* **18** 556
Curzon A E and Pawlowicz A T 1965 *Proc. Phys. Soc. London* **85** 375
[4] Jordan T H, Streib W E, Smith H W and Lipscomb W N 1964 *Acta. Crystallogr.* **17** 777
Cox D E, Samuelsen E J and Beckurts K H 1973 *Phys. Rev.* B **7** 3102
[5] de Fotis G C 1981 *Phys. Rev.* B **23** 4714
Meier R J, Schinkel C J and A. de Visser 1982 *J. Phys. C: Solid State Phys.* **15** 1015
[6] Collins M F 1966 *Proc. Phys. Soc. London***89** 415
Alikhanov R A, Ilyina I L and Smirnov L S 1972 *Phys. Status Solidi* **50** 385
Meier R J and Helmholdt R B 1984 *Phys. Rev.* B **29** 1387
Leoni F and Sacchetti F 1973 *Phys. Rev.* B **7** 3112
[7] Deraman M, Dore J C and Schweitzer J 1985 *J. Magn. Magn. Mater.* **50** 178
Dunstetter F, Plakhti V P and Schweizer J 1988 *J. Magn. Magn. Mater.* **72** 258
Dunstetter F, Plakhti V P and Schweizer J 1991 *J. Magn. Magn. Mater.* **96** 258
Stephens P W and Majkrzak C F 1986 *Phys. Rev.* B **33** 1
[8] Klein M K, Levesque D and Weiss J J 1980 *Phys. Rev.* B **21** 5785
[9] Martinez J L, Bermejo F J, Garcia-Hernandez M and Mompean F J 1991 *J. Phys.: Condens. Matter* **3** 3849
Chahid A, Bermejo F J, Martinez J L, Mompean F J and Garcia-Hernandez M 1992 *Physica* **B180–181** 843
[10] Chahid A, Bermejo F J, Garcia-Hernandez M, Enciso E, Martinez J L 1992 *Europhys. Lett.* **20** 71

[11] Chahid A, Bermejo F J, Enciso E, Garcia-Hernandez M and Martinez J L 1992 *J. Phys.: Condens. Matter* **4** 1213
[12] Lovesey S W 1986 *Theory of Neutron Scattering from Condensed Matter* vol 2 (Oxford: Oxford Science Publications)
[13] Kleiner W H 1955 *Phys. Rev.* **97** 411
Stephens P W 1985 *Phys. Rev.* B **31** 4491
[14] Kobashi K, Klein M and Chandrasekharan V 1979 *J. Chem. Phys.* **71** 843
[15] Laufer J C and Leroi G E 1971 *J. Chem. Phys.* **55** 993
[16] Powles J G and Gubbins K E *Chem. Phys. Lett.* **38** 405
[17] Allen M P and Tildesley D J 1987 *Computer Simulation of Liquids* (Oxford: Clarendon)
[18] Johnson M W 1974 Atomic Energy Research Establishment Report No 7682
[19] Rieutord F Institut Laue–Langevin (private communication)
[20] On formal grounds only the case of an incoherent monoatomic system or that of a set of harmonic oscillators enable the estimation of the $Z(E)$ generalized frequency distribution from the measured spectra. A knowledge of the rotational and spin dynamics is needed to account for these effects when extrapolating the spectra to the hydrodynamic limit.
[21] Dore J C, Walford G and Page D I 1975 *Molec. Phys.* **29** 565
see also
Clarke J H, Dore J C and Sinclair R N 1975 *Molec. Phys.* **29** 581
[22] Evans M, Evans G, Coffey W T and Grigolini P 1982 *Molecular Dynamics and Theory of Broadband Spectroscopy* (New York: Wiley) p 360
[23] Levesque D and Weiss J J 1975 *Phys. Rev.* A **12** 2584
[24] Bezugly P A, Tarasenko L M and Yu.Ivanov S 1969 *Sov. Phys.–Solid State* **10** 1660
[25] Clouter M J and Kiefte H 1973 *J. Chem. Phys.* **59** 2533
see also
Kiefte H and Clouter M J 1975 *J. Chem. Phys.* **62** 4780 and references therein
[26] A simple calculation of the $J(Q,\omega)$ functions using the parameter values given in previous sections for the mass-diffusion and reorientational motions using rotational-diffusion approximations will reveal that the shape of the calculated function does not show any peak within the energy-transfer range of interest. On the contrary, such parameters will give rise to smooth curves with a very flat maximum centred well above 15 meV.
[27] Collins M F and Marshall W 1967 *Proc. Phys. Soc.* (London) **92** 390
[28] Lovesey S W and Meserve R A 1973 *JPC* **6** 79
[29] Cuccoli A, Tognetti V, Lovesey S W 1990 *JPCM* **2** 3339
see also
Young A P and Sastry B S 1982 *JPC* **15** 4547
[30] Lovesey S W 1986 Megann A *Z. Physik.* **B63** 437
[31] Brodynaskii A P and Freeman Yu A 1985 *Sov. J. Low Temp. Phys.* **11** 714
[32] Westhead D R, Cuccoli A, Lovesey S W and Tognetti V 1991 *J. Phys.: Condens. Matter* **3** 5235
[33] Meier R J 1984 PhD Dissertation, University of Amsterdam
[34] The numerical values given in [33] p 57 were approximated by means of $J(r) = J_0 \exp(-\alpha(r-r_0))$ with $J_0 = -90$ K, $\alpha = 4.13$ and $r_0 = 3.012$ Åfor an interval $3.1 < r < 3.7$. The tabulated function changes the sign of the exchange-coupling constant for distances larger than 3.8 Åand therefore a more complicated representation is needed. A polynomial representation was used to interpolate the data.
[35] Gerling R W and Landau D P 1990 *Phys. Rev.* B **42** 8214
[36] Fagerstroem C H and Hallis A C-Hallet 1969 *J. Low Temp. Phys.* **1** 3
[37] For a homonuclear diatomic molecule the correlations $\langle v_{COM}(t) \cdot \omega(0) \rangle$ vanish, and therefore only higher-order mixed autocorrelations contain information regarding this topic. The amount of coupling in the liquid phase was established from the simulation by Weis J J and Levesque D, *Phys. Rev.* A **13** 450 (1976). No difference was found in the liquid between the COM and total structure factors for wavevectors below ≈ 11 Å^{-1}. Some data concerning condensed (glassy) nitrogen are given in Evans M, Evans G and Davies R, *Adv. Chem. Phys.* **44** 255 (1980).
[38] Storchak V G, Kirilov B F, Pirogov A V, Duginov V N, Grebinnik V G, Lazarev A B, Ols'shevsky V G, Pomyakushin V Yu, Shilov S N and Zhukov V A 1992 *Phys. Lett.* A **166** 429
[39] Wormer P E S and van der Avoird A 1984 *J. Chem. Phys.* **81** 1929
[40] Dunstetter F 1988 PhD dissertation, Universite de Paris-Sud